Single Wall Carbon Nanotube (SWCNT) Devices as THz Detectors and Mixers

Enrique Carrion**, Martin Muthee**, Zuojing Chen, John Nicholson, Eric Polizzi, and Sigfrid Yngvesson

Department of Electrical and Computer Engineering, Univ. of Massachusetts, Amherst, MA01003, USA

*Contact: ecarrion@ecs.umass.edu, yngvesson@ecs.umass.edu; phone (US)(413)545-0771

** These authors contributed equally to this paper

***Abstract*—In this paper we present a review of the progress that our group has done in the development of Carbon Nanotube based devices as THz detectors. We describe new techniques for fabrication of log periodic antennas, as well as for better control of the placement and selection of the CNTs. The new THz detector devices utilize single tubes (or a few single tubes in parallel), and have potential for increased responsivity by about two orders of magnitude, compared with the devices based on CNT bundles that we reported on at the ISSTT 2009. The new devices are initially characterized being characterized as microwave detectors in order to study and optimize the two detection modes ("diode"-type, and bolometer type) that we have identified. We plan to utilize the best CNT devices as heterodyne detectors, down-converting in a two-laser experiment from different terahertz frequencies to the GHz range. Further, we present new results of time-dependent simulations of the THz response of a single carbon nanotube. We use time-dependent density functional theory and obtain a value for the kinetic inductance that agrees with accepted theoretical/experimental values**

I. INTRODUCTION

Our first paper at the **ISSTT** symposia on the topic of Terahertz detection in carbon nanotubes (CNTs) was presented at **ISSTT2005** [1]. We also discussed the topic of microwave and terahertz detection in CNTs in ref. [2], as well as a later ISSTT symposia. Our group reported the first terahertz detection in bundles containing m-SWCNTs [3], up to 2.5 THz, at ISSTT2008 and ISSTT2009. The SWCNT bundles were coupled to log-periodic antennas similar to those used to couple to NbN HEBs. CNTs are a promising medium for future terahertz detectors based on some general features based on their small diameters (1-2 nm) which lead to very low heat capacity and low capacitance. They can also have nearly ideal transport properties (ballistic transport) for both electrons and phonons. Detection in m-SWNTs can occur due to two basic mechanisms: (1) *a diode type* mechanism demonstrated at microwaves in [4]-[10]; (2) *bolometer type* modes, similar to that in HEBs and other terahertz bolometers. Both types of modes will be discussed below. We present advances in device fabrication that have enabled us to realize antenna-coupled SWCNT devices that contain a single SWCNT, or just a few SWCNTs. We have demonstrated excellent microwave detection in such tubes, and discuss how these results can be translated to enable realization of future terahertz SWCNT detectors with enhanced responsivity. We also present unique results from time-dependent simulations of the THz response of SWCNTs, relevant for the development of such detectors.

II. DEVICE FABRICATION

As described at earlier ISSTT symposia, we fabricated the CNT devices by the dielectrophoresis (DEP) method. We refer to [11] and our earlier ISSTT papers for a general description of the method. We employed two types of log-periodic toothed antennas, fabricated by lift-off UV lithography in sputtered films of either gold or palladium, see Figure 1. The latest antennas utilize e-beam evaporation for the gold film deposition. In the initial stages of working out optimized processes for DEP we often employed standard low-resistivity silicon substrates. We then changed to high-resistivity substrates for actual devices to test at microwaves or at terahertz. All silicon substrates were oxidized with typical oxide thickness of 350 nm.

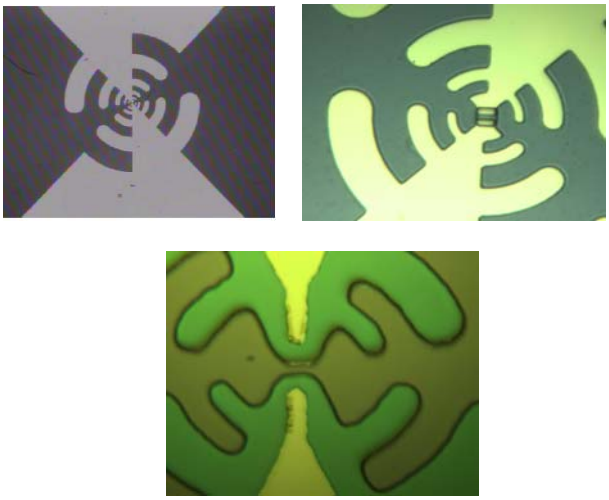

Figure 1. Different terahertz log-periodic antennas used in this work: LPA2 (top left); LPA3 (top right) and LPA4 (bottom).

Antenna LPA2 (Figure 1, top left) has a 1 μm gap and an estimated upper frequency limit of 3.5 THz. The LPA2 design is identical to one we used in our earlier NbN HEB work [12]. We were also concerned about minimizing the thermal conductance, and therefore fabricated antennas that had an etched trench in the silicon oxide in the gap region. Antennas of type LPA2 were employed as etching mask for

RIE etching of the trench. We term LPA2 antennas with a trench "LPA3". Antenna LPA4 is a new design that was employed to facilitate DEP deposition of tubes with improved contacts, see Figure 1 (bottom). In one version, an antenna with about a 9 μm gap (but without "side teeth"; yellow in Figure 1) was first fabricated and DEP was performed to place tubes in its well-defined gap. A second (log-periodic) antenna (green in Figure 1) was then aligned and fabricated on top of the first one, thus establishing *contact from the top side* of the CNTs. Typically, the bottom antenna was made from gold and the top one from palladium. Palladium is known to produce the best contacts to CNTs, especially when it is applied from the top, and we have confirmed this in our work. A different version of LPA4 was later fabricated by using the same mask (the one with the smaller gap in Figure 1) for both the bottom and the top antenna. The photo resist for the top antenna was exposed differently which produced an antenna with a smaller gap that overlapped that of the bottom antenna along all edges.

Results from our earlier work are shown in Figure 2. During this period we employed CNTs that were present in bundles, even after long ultrasonication [13]. The bundles also contained a surfactant, that affects the quality of the contacts negatively. The SEM pictures show how the edges of the antennas were "flaked up" which made DEP difficult to perform successfully. Another problem at this stage was that the tubes were deposited outside the main gap of the antennas. Attempt to avoid this by etching a window over that gap (as shown in Figure 2, top left) and then performing DEP were only partially successful, but should succeed after further experimentation.

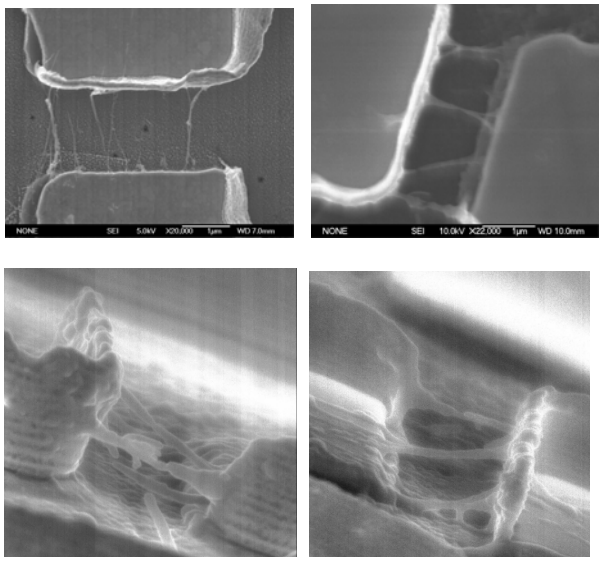

Figure 2. SEM pictures of devices with CNT bundles, using antenna LPA2. The bottom pictures are taken at a slanted angle to show the etched trench below the bundles, as well as the flaking of the gold edges.

The IV-curves of all bundle devices were of the "Zero-Bias Anomaly (ZBA) type, and dominated by the contacts, as described in our earlier papers (see Figure 3).

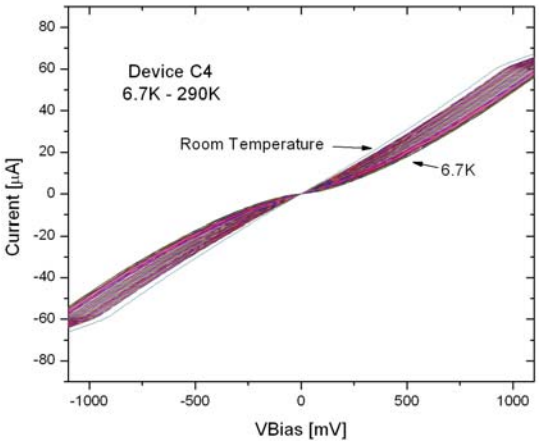

Figure 3. IV-curves for a typical CNT bundle device.

To fabricate single tube devices with better contacts we switched to a different CNT manufacturer [14]. These tubes had been dispersed in water effectively by the manufacturer and did not include any surfactant. The procedures for the DEP were re-optimized in order to emphasize single tubes with good contacts. Important elements in the new process are the use of a very low concentration of the tubes in the solution (ng/mL), and selection of an antenna gap that matches only the longest of the tubes in the solution. While other methods have also been employed elsewhere for placing single SWCNTs on contacts, we believe the method described here is unique, and relatively simple to implement. We monitor the DC resistance simultaneously through a bias tee. The DEP process is halted when the dc resistance is sufficiently low. All devices were annealed in air at 200 ^{o}C for two hours which decreased the contact resistance. As the result of the improved DEP process we were able to contact single SWCNTs to the LPA4 antenna. An example (device F2) is shown in Figure 4. The tube was measured by AFM to have a diameter of 1.5 nm, clearly identifying it as a single tube. We also note that DEP preferentially aligns metallic tubes, as versus semiconducting ones, which was confirmed based on the IV-curves for our devices.

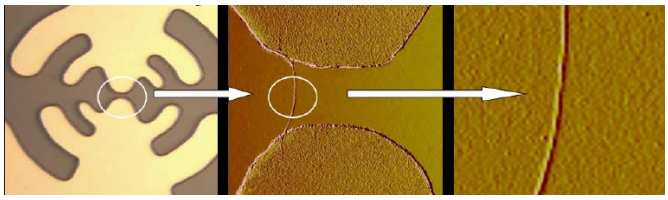

Figure 4. Example of a single SWCNT, contacted to an LPA4 antenna. The two frames in the center and to the right were imaged in an AFM.

Even though the SWCNT in the device in Figure 4 was placed from the top of the antenna contacts, it had improved contact resistance as shown by an IV-curve that "saturated" at higher voltages, see Figure 5. The saturation occurs because most of the bias voltage is developed across the SWCNT, rather than just the contacts, in this case. The resistance increases at higher voltages due heating of the

electrons in the tube and consequent optical phonon emission.

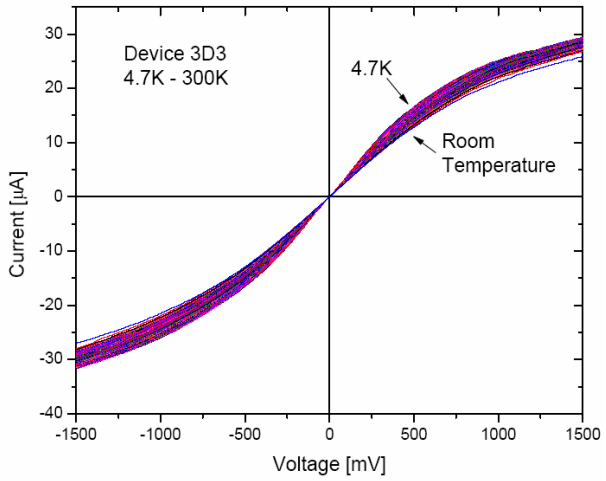

Figure 5. IV-curves at temperatures from 4.7 K to 300 K for device 3D3.

Further improvement of the contact resistance has been achieved by implementing the bottom/top antenna method described above. Figure 6 shows an IV-curve at 300 K for a device of this type, fabricated very recently.

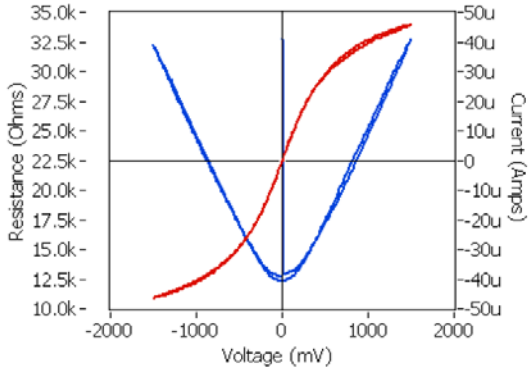

Figure 6. IV-curve (red) and resistance versus voltage (blue) for a device made with a bottom gold LPA4 antenna and a top palladium LPA4 antenna. The device was measured at 300 K.

III. FURTHER DC DEVICE CHARACTERIZATION

We performed further measurements of the device resistance versus temperature in order to explore the height of the contact barriers. In the AFM picture of Figure 7 we can identify one single tube and one bundle, containing two tubes. The resistance of this device while varying both the bias voltage and the temperature is displayed in a 3-D diagram in Figure 8. It is clear that there are two regions: (i) for low T and low V, the contact resistance begins to dominate; (ii) for higher T and V the contact resistance plays only a minor role. This type of studies are being used to optimize the device processing in the direction of pushing the contact effects toward lower T/V. For this particular device, the contact resistance may be neglected above about 200 K. The best low barrier contact devices we are aware of fabricated by other groups have negligible contact resistance effects above about 20 K [5,6,15].

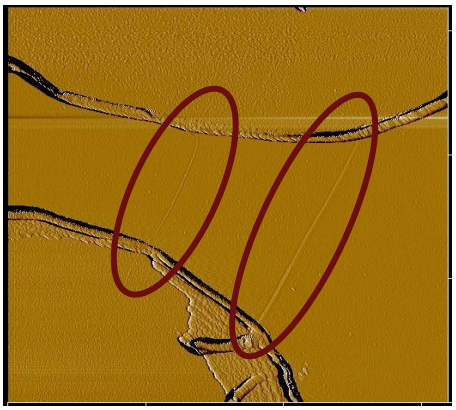

Figure 7. AFM picture of device 3D3

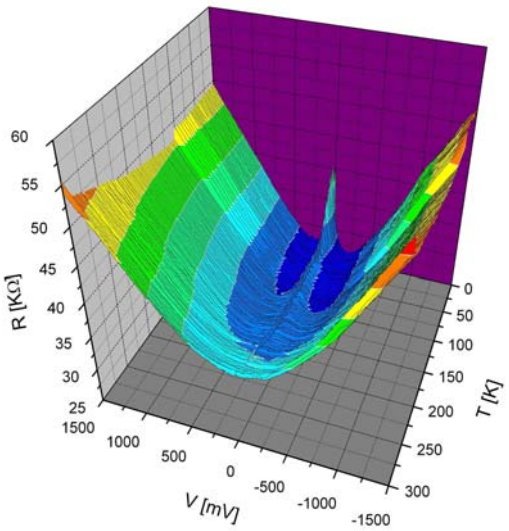

Figure 8. A 3-D plot of the resistance vs bias voltage and temperature for device 3D3.

IV. MICROWAVE DETECTION MEASUREMENTS

Microwave (MW) detection in the devices was measured by feeding a MW signal through a coaxial cable to the device, which was mounted in a liquid helium dewar. This method allows us to perform both microwave and terahertz measurements on a particular device without changing the setup. Our experimental setup was described in our previous ISSTT papers. We identified two different processes for MW detection:

(1) *The "diode" process*. This detection mode is similar to that occurring in any semiconductor diode, except for the trivial difference that our IV-curves are symmetric between positive and negative bias voltages. As in our previous work, we model the SWCNT as shown in Figure 9.

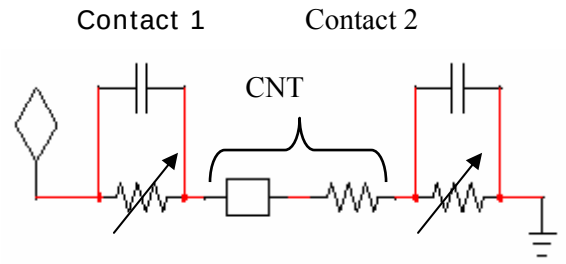

Figure 9. The circuit model for a single SWCNT.

In the diode mode, we utilize the nonlinearity of the contact resistances in Figure 9, the IV-curve for the entire device is well described by this model, while neglecting the intrinsic SWCNT resistance. These IV-curves are similar to the ones in Figure 3). We find the responsivity from:

$$S_V = (1/4)R\frac{d^2I}{dV^2}\frac{V_{MW}^2}{P_{MW}} \qquad (1)$$

Here, R = V/I is the device resistance at the operating point, V_{THz} is the MW voltage at the device terminals and P_{THz} is the available power from the MW source. S_V has units of V/W.

2) For the *bolometer mode*, the expression is

$$S_V = \frac{V_0 * b}{G_{th}} \qquad (2)$$

where V_0 is the bias voltage, b = (1/R)(dR/dT) and G_{th} the thermal conductance. As shown in Figure 10, the diode mode occurs in the lowest voltage range, and the bolometer mode at higher bias voltages.

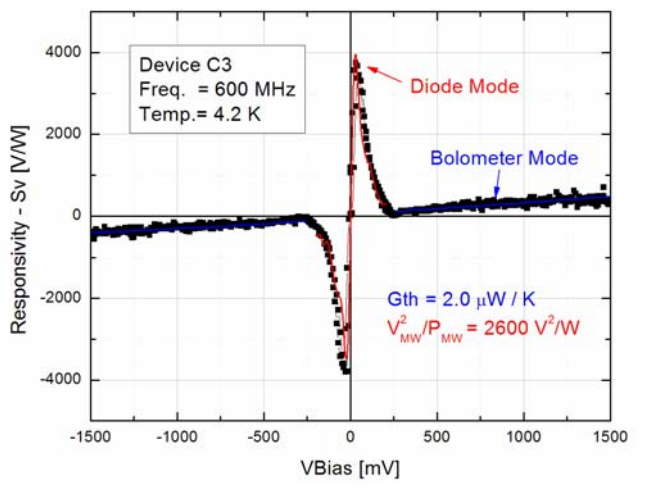

Figure 10. Responsivity versus bias voltage for device C3 at 4.2 K.

The device in Figure 10 has one the highest responsivities for either mode, about 4,000 V/W in the diode mode and 500 V/W in the bolometer mode. The response is quite flat with frequency up to 3 GHz, the highest frequency of the source used at the moment. We can predict the *ideal response* in the bolometer mode from Eq. (2), using R(T) and G_{th} for an optimum device [5,6,15], see Figure 11.

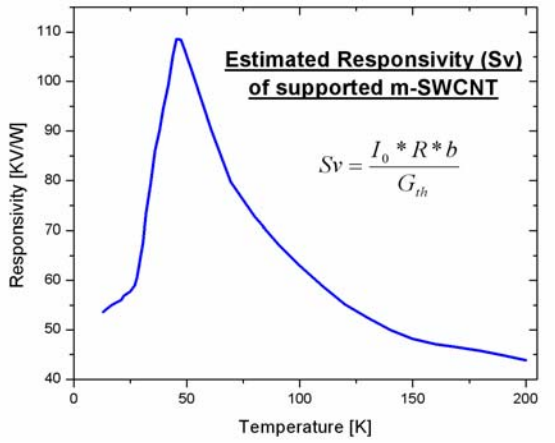

Figure 11. Predicted optimum responsivity for a single CNT in the bolometer mode.

What is noteworthy in Figure 11 is the fact that the responsivity depends only very slowly on the temperature, at least up to 200 K. For a more realistic device, we must include estimated coupling losses due to the high resistance of the device, 18 dB, which reduces the maximum S_V to about 2,000 V/W. This excellent responsivity should also occur at terahertz frequencies provided that the coupling loss were the same. We will discuss the THz coupling loss further below. The measured MW responsivities for devices C3 (Figure 10) and F2 agree well with this theory. The maximum responsivity (500 V/W) is less than for the optimum device primarily because the contact barriers are higher. MW measurements of the type described here enable us to optimize the device fabrication, particularly in terms of the contact barriers, as reflected in the IV-curves.

We plan to perform heterodyne measurements using two lasers for a device that has been optimized in this manner. We can estimate the conversion gain (G_C) in the heterodyne mode from the responsivity in the direct detector mode [17]:

$$G_C \approx 2S_V^2 P_{LO} / R_L \qquad (3)$$

Here, P_{LO} is the local oscillator power and R_L the load resistance at the IF. With even a moderately good S_V = 1,000 V/W, $P_{LO} = 10^{-6}$ W, and R_L = 100 Ω, we estimate a conversion gain of -17 dB. **Since the responsivity can potentially be much higher the prospects for realizing a very efficient mixer are excellent. Moreover, the predicted temperature dependence of the responsivity (Figure 11) is very slow, showing the potential for operation at least up to about 100K.** Eq. (3) assumes that the IF output is matched to the IF amplifier and this would require a matching circuit. Alternatively, some IF mismatch

may be tolerated, or for example traded against using higher LO power.

An estimate of the LO power can best be obtained by using the already measured typical IV-curves. We find a P_{LO} of about 1 μW or less.

V. TERAHERTZ COUPLING TO SWCNTS

We have simulated the coupling loss for an m-SWCNT, expressed in terms of the S-parameter S11 in dB, using a circuit model similar to that in Figure 9. The tube was assumed to be 1 μm long. The circuit model assumes a particular version of the Luttinger-Tomonaga plasmon model, which as mentioned earlier is not yet experimentally verified. Questions related to the terahertz model for SWCNTs and the resulting coupling loss are the most significant questions that still require much research in the filed of terahertz SWCNT detectors. It is encouraging to note that substantially reduced coupling loss is predicted at the plasmon resonance frequencies based on our present understanding of such models.

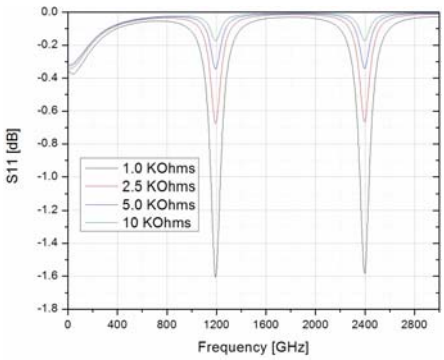

Figure 12. Simulated coupling loss for a metallic SWCNT at THz frequencies. Four different values for the SWCNT intrinsic resistance were assumed, as marked.

VI. TIME-DEPENDENT DFT SIMULATIONS

Another objective of this study consists in performing reliable modeling and simulations of the CNT electron dynamics in order to supplement the high-frequency electronics experiments. Our primary focus has been concerned with setting up a robust and efficiency time-dependent density functional theory (TDDFT) simulation-based framework which we can address the numerical challenges arising from large scales related to both space and time.

For addressing the electronic structure calculations of large-scale atomistic systems such as long CNTs, we have proposed a new modelling approach which benefits from well-suited combinations of specific mathematical and numerical algorithms that exploit fully the potentiality of real-space mesh techniques in achieving linear scaling performance [18]. As compared to traditional approaches, our DFT technique applied to CNTs allows order of magnitude speed-up and is applicable to both pseudopotential approaches and all-electron calculations. To address the problem of long time period required to capture the behavior of the electron dynamics in the THz regime, we have developed a numerical procedure that goes beyond perturbation theory or linear response. Accurate, robust and scalable time dependent simulations are indeed difficult, if not impossible, to achieve using conventional modeling approaches. Our technique consists of performing directly the integration of the time evolution operator (i.e. time ordered exponential) along with the spectral decomposition of the time dependent Hamiltonian at each time step. The expression of the evolution operator is given as follows:

$$\psi(t) = \hat{U}(t,0)\psi_0 = \mathcal{T}\ \exp\left\{-i\int_0^t d\tau \hat{H}(\tau)\right\}\psi_0$$

Our in-house FEAST eigenvalue solver [19,20] (which is more efficient and scalable than other conventional eigenvalue solvers) can be used to speed up the spectral decompositions and evaluate the exponential at each small time step $d\tau$. In our work [21], we have also proposed a new Gaussian quadrature scheme to minimize the integration error on the Hamiltonian. This scheme provides a good trade off between computational consumption and numerical accuracy, meanwhile unitary, stability and time reversal properties are well preserved.

Here, we are applying this TDDFT framework to the simulation of a (5,5) CNT whose end sections are wrapped around two electrodes, with no charge transfer, producing an AC voltage at the THz frequency (see Figure 13).

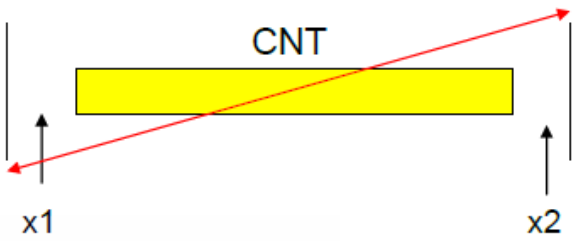

Figure 13. Simulation set-up with an isolated CNT in contact with two electrodes (no charge transfer) producing an AC voltage at the THz frequency.

The time variation of the electron density calculated at the two specific positions x1, x2 in Figure 13 is represented in Figure 14.

We estimate the kinetic inductance (L_K) of this tube from the basic definition that sets ½ $L_K I^2$ equal to the kinetic energy. The latter can be obtained directly from our simulation. The kinetic inductance we find this way is 3.6pH/nm which is in agreement with experimental and theoretical estimation results of 8pH/nm [22] and 4pH/nm [16]. We note that the kinetic inductance is an important circuit parameter in the transmission line model in Figure 9, that was referred to in our discussion of the plasmon phenomena in SWCNTs.

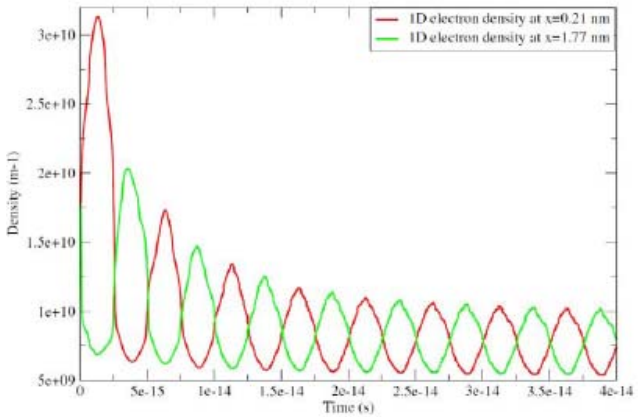

Figure 14. Time variation of the cross-sectional average of the electron density obtained at positions x1, x2. The CNT is only 2nm long here, and after a few periods the signal becomes periodic.

ACKNOWLEDGEMENT

This work was supported by grants from the US National Science Foundation, grant numbers ECS-0508436 and ECS-0725613.

REFERENCES

[1] K.S. Yngvesson, "A New Hot Electron Bolometer Heterodyne Detector Based on Single-Walled Carbon Nanotubes," *16th Intern. Symp. Space Terahertz Technol.*, Gőteborg, Sweden, May 2005, p. 531.

[2] K.S. Yngvesson, "Very wide bandwidth hot electron bolometer heterodyne detectors based on single-walled carbon nanotubes," *Applied Phys. Lett,* vol. **87**, p. 043503 (2005).

[3] K. Fu, R. Zannoni, C. Chan, S.H.Adams, J. Nicholson, E. Polizzi and K.S. Yngvesson, "Terahertz detection in single wall carbon nanotubes," *Appl. Phys. Lett.*, **92**, 033105 (2008). For further details, see K. Fu, "Metallic Carbon Nanotubes, Microwave Characterization and Development of a Terahertz Detector," *M.Sc. thesis, University of Massachusetts, Amherst, MA* (2008).

[4] F. Rodriguez-Morales, R. Zannoni, J. Nicholson, M. Fischetti, K. S. Yngvesson, and J. Appenzeller, *Appl. Phys. Lett*. **89**, 083502 _2006_.

[5] D.F. Santavicca and D. Prober, "Terahertz Resonances and Bolometric Response of a Single Walled Carbon Nanotube", paper 1646, 33rd Intern. Conf. Infrared, Millimeter and Terahertz Waves, Sept. 2008, CalTech, Pasadena, CA.

[6] D.F. Santavicca, J. Chudow, A. Annunciata, L. Frunzio, D. Prober, M. Purewal and P. Kim, "Terahertz resonances on a single-walled carbon nanotube," Intern. Workshop on Optical Terahertz Science and Technol., Santa Barbara, CA, March 7-11, 2009. Also, see D.F. Santavicca, Ph.D. Thesis, Yale Univ., Dec. 2009.

[7] H.M. Manohara, E.W. Wong, E. Schlecht, B.D. Hunt, and P.H. Siegel, *Nano Lett.* **5**, 1469 (2005).

[8] S. Rosenblatt, H. Lin, V. Sazonova, S. Tiwari, and P.L. McEuen, *Appl. Phys. Lett*. **87**, 153111 (2005).

[9] A. A. Pesetski, J.E. Baumgardner, E. Folk, J. Przybysz, J. D. Adam, and H. Zhang, *Appl. Phys. Lett.*, **88**, 113103 (2006).

[10] M. Tarasov, J. Svensson, L. Kuzmin, and E. E. B. Campbell, *Appl.Phys.Lett.*, **90**, 163503 (2007).

[11] R. Krupke and F. Hennrich, *Adv. Eng. Mater.* **7**, 111 _2005.

[12] E. Gerecht, C. Musante, Y. Zhuang, K. Yngvesson, T. Goyette, J. Dickinson, J. Waldman, P. Yagoubov, G. Gol'tsman, B. Voronov, and E. Gershenzon, *IEEE Trans. Microwave Theory Techn.*, vol. **47**, pp. 2519–2527, (1999).

[13] Cheap Tubes, Brattleborough, VT, USA.

[14] CNTRENE from Brewer Science, Rolla, MO, USA.

[15] M. S. Purewal, B. H. Hong, A. Ravi, B. Chandra, J. Hone, and P. Kim, "*Scaling of Resistance and Electron Mean Free Path of Single-Walled Carbon Nanotubes*", *Phys.Rev.Lett*. **98**, 186808 (2007).

[16] P. J. Burke, "*Lüttinger Liquid Theory as a Model of the Gigahertz Electrical Properties of Carbon Nanotubes,*" IEEE Trans. Nanotechnol. **1**, 129 (2002).

[17] B.S. Karasik and A.I. Elantiev, Proc. 6th Intern. Symp. Space Terahertz Technol., Pasadena, CA, March 1995, pp. 229-246.

[18] D. Zhang, E. Polizzi, *Linear scaling techniques for first-principle calculations of large nanowire devices,* 2008 NSTI Nanotechnology Conference and Trade Show. Technical Proceedings, Vol. 1 pp12-15 (2008).

[19] E. Polizzi, *Density-Matrix-Based Algorithms for Solving Eingenvalue Problems,* Phys. Rev. B. Vol. 79, 115112 (2009).

[20] *http://www.ecs.umass.edu/~polizzi/feast*

[21] Z. Chen *Efficient modeling techniques for time-dependent quantum system with applications to Carbon nanotubes*,. MS thesis, UMass Amherst (2010).

[22] Zhang, M., Huo, X., Chan, PCH, Liang, Q., and Tang, ZK. *Radio-frequency transmission properties of carbon nanotubes in a field-effect transistor configuration.* IEEE Electron Device Letters 27, 8, 668-670 (2006).